Demonstration of Enhanced Optical Pressure on a Structured Surface

Li-Fan Yang, Anurup Datta, Yu-Chun Hsueh, Xianfan Xu, and Kevin J. Webb[*]

Purdue University, West Lafayette, Indiana 47907, USA

The interaction of electromagnetic waves with condensed matter and the resultant force is fundamental in the physical sciences. The maximum pressure on a planar surface is understood to be twice the incident wave power density normalized by the background velocity. We demonstrate for the first time that this pressure can be exceeded by a substantial factor by structuring a surface. Experimental results for direct optomechanical deflection of a nanostructured gold film on a silicon nitride membrane illuminated by a laser beam are shown to significantly exceed those for the planar surface. This enhanced pressure can be understood as being associated with an asymmetric optical cavity array realized in the membrane film. The possible enhancement depends on the material properties and the geometrical parameters of the structured material. Such control and increase of optical pressure with nanostructured material should impact applications across the physical sciences.

It has been more than a century since the radiation pressure experiments confirmed that light can impart a mechanical force on matter [1,2], in a manner consistent with the prediction of Maxwell [3]. More recently, the laser tweezing work of Ashkin and others [4,5] has led to instruments that are important for molecular biology [6]. Optical atom traps have also been studied extensively for realizing condensates and achieving precise clocks [7–9]. We demonstrate that the optical force on a material is sensitive to the surface structure and show that the pressure can be substantially larger than on a planar surface. By measuring the deflection of a membrane having a patterned metal surface, shown schematically in Fig. 1(a), we present experimental confirmation of the enhanced pressure on a surface that was previously proposed [10]. The physical basis of the enhancement is an asymmetric resonant cavity array that provides for an increase in the net pressure. In this way, the structured surface is increasing the pressure by providing a further nanometer-scale spatial dimension for the interaction of the light with the material.

The pressure on a mirror can be understood at the atomic level, where there is a momentum exchange between the photon and the atom that can be influenced by the environment [11]. At the macroscopic material level, the optical force on a surface has been described by a pressure [2,3]

$$P = \frac{S(1 + |\Gamma|^2)}{v}, \qquad (1)$$

where S is the time-averaged normally incident Poynting vector magnitude (W/m^2), Γ is the field reflection coefficient, and v is the wave velocity in the background, assumed to be c, the speed of light in vacuum, in this work. Consequently, the maximum pressure from Eq. (1) is

$P = 2S/c$ N/m^2. However, Eq. (1) precludes information on how the field interacts with the material. A fundamental approach is to describe the optical force density in the material in terms of fields. Assuming $\exp(-i\omega t)$ time dependence with source-free dielectric media, this can be written as [12]

$$\langle \mathbf{f} \rangle = \frac{\omega \mu_0}{2} \Im\{\mathbf{P} \times \mathbf{H}^*\} + \frac{1}{2}\Re\{(\mathbf{P} \cdot \nabla)\mathbf{E}^*\}, \qquad (2)$$

where $\langle \mathbf{f} \rangle$ (N/m^3) is the time-averaged force density, $\mathbf{P}$ is the homogenized polarization, $\mathbf{H}$ is the magnetic field intensity, $\mathbf{E}$ is the electric field intensity, μ_0 is the free space permeability, $\Im\{\cdot\}$ is the imaginary part, $\Re\{\cdot\}$ is the real part, and peak field amplitudes are assumed. The more
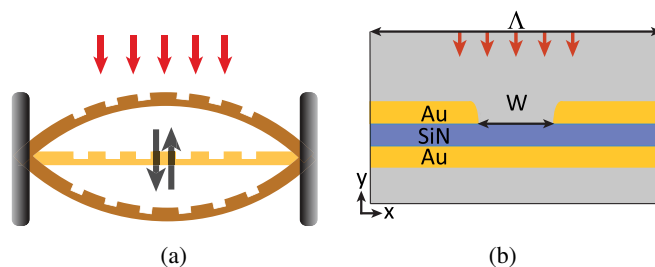

FIG. 1. (a) The structuring of the surface of a metal film with an array of resonant cavities can result in an increase in the optical pushing and pulling force (black arrows), relative to that on a perfect mirror and a planar surface. The red arrows indicate the direction of the incident light. (b) Simulated structure with a periodic boundary (left and right) and parameters: period Λ, slot width W, gold (Au) thickness 50 nm, and silicon nitride (SiN) thickness 50 nm. We consider deflection with a laser having a free space wavelength of 1070 nm.

general form of Eq. (2) has been used to describe key experiments [13,14], is consistent with a development from Einstein and Laub [15], and results in the theory of Lorentz in the static limit [16]. Solving for the fields in a planar gold (Au) mirror with plane wave illumination using Eq. (2), where the second term is zero with normal illumination, leads to the force density and hence a pressure that is very close to that from Eq. (1) with $|\Gamma| = 1$. This pressure on a planar surface thus provides a good reference for the results we present. While Eq. (1) provides a reasonable description for the force on a planar surface with no transmission, Eq. (2) allows the 3D structured material situation to be treated, where both the cross and gradient terms contribute to the pressure with a structured material.

We use a 50 nm thick silicon nitride (SiN) membrane coated with 50 nm of Au on both sides and guidance from a 2D numerical (finite element method) field solution of the periodic geometry in Fig. 1(b) [17], with an incident plane wave having a free space wavelength of 1070 nm. The force density in the material from Eq. (2) is integrated over the unit cell area (x-y plane), and the pressure is obtained by normalizing with the invariant z direction and the unit cell width (Λ). Two degrees of freedom were considered, the period (Λ) and the slot width (W). An elliptical slot taper (a consequence of the fabrication process) was used with an axial ratio of $\sqrt{3}$, the Au thickness divided by the taper width at the SiN interface. This was obtained from a fit to scanning electron micrograph (SEM) image data for fabricated structures. Consequently, the slot width at the top is larger than W by the corresponding amount. The dielectric constant for Au assumed is $-49.05 + i3.65$ [18], and that for the SiN membrane was obtained as 3.94 from an ellipsometer measurement. Simulations with an incident power density of 318 MW/m^2 (about 1 mW in a 2 μm diameter beam) show the optical force character of the three slot arrays fabricated as being strong push (25.7 N/m^2), strong pull (-20.2 N/m^2), and weak push (3.26 N/m^2) (see Ref. [19], which includes Refs. [10,20]), specifically designed to allow demonstration of enhanced pressure relative to the planar case (2.11 N/m^2). The physical basis for specific pressures of these slot arrays is described based on simulated results [19].

The slot arrays were formed in an Au coating on a SiN membrane (50 nm, Norcada, Inc.). The suspended square membrane had dimensions of 500×500 μm^2 and was supported from four sides on a Si frame of thickness 200 μm. Gold of thickness 50 nm was deposited on both sides of the membrane using an electron-beam evaporator (CHA), following deposition of a 5-nm layer of titanium for adhesion. Thus, for practical purposes, a three-layered symmetric membrane structure made of Au-SiN-Au was formed. Focused ion beam (FIB) milling (FEI Nova 200) was used for fabrication of the slots on the bottom, recessed side of the structure (with a 10 pA current). Three periodic slot array structures were milled near the center of the
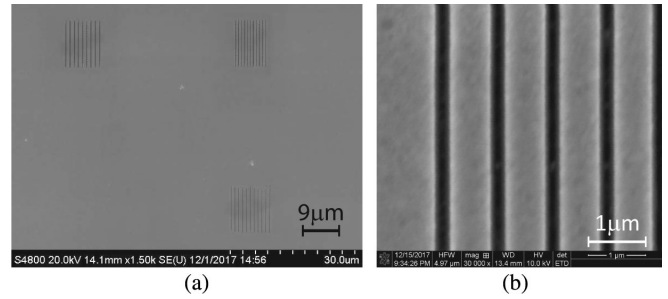

FIG. 2. (a) The three slot arrays with an enhanced optical force: strong push, top left; strong pull, top right; and weak push, bottom right. SEM image data indicate that all slots have a length of 11.5 μm; for the strong push structure, 9 slots with $W = 250 \pm 2.2$ nm, $\Lambda = 966.4 \pm 7.7$ nm; for the strong pull structure, 11 slots with $W = 200.4 \pm 3.4$ nm, $\Lambda = 692.2 \pm 7.3$ nm; and for the weak push structure, 11 slots with $W = 124 \pm 3.3$ nm, $\Lambda = 886 \pm 9.8$ nm. (b) A higher-magnification SEM image of the strong push slot array.

membrane with nominal dimensions corresponding to those used in the simulations [19] and measured dimensions indicated in the caption of Fig. 2. The SEM image for these slot arrays is shown in Fig. 2(a). A fourth symmetric location was used for the planar deflection data. A magnified image of the large pushing force structure [top left of Fig. 2(a)] is shown in Fig. 2(b). Images from an SEM (Hitachi S-4800) with an edge detection method that defines the edges from the local maximum gradient of the image intensity [21] provided precise geometry information for the fabricated structures for analysis and extraction purposes.

The membrane was mounted on a glass slide with a hole to allow the 1070 nm force laser beam to directly illuminate the structured Au surface formed on the back of the membrane. As Fig. 3(a) illustrates, the intensity-modulated (mechanically chopped at 220 Hz) force laser illuminated the bottom, structured side of the membrane and a 640 nm sensing laser, positioned on the other (nonpatterned) side and directly opposite the force laser, allowed the membrane deflection to be monitored by measurement of the current from a four-quadrant detector. The specifics of the experiment are shown in Fig. 3(b). Measurement of the deflection signal at the chopping frequency with a lock-in amplifier (Zurich Instruments HF2) removes any deflection bias due to the sensing laser. By calibrating to a known displacement with a piezoelectric stage (Thorlabs PE4), we determined that the sensitivity of the lock-in amplifier led to a displacement accuracy of 0.35 nm, setting the lower bound for the results we show.

The data we present are from a single set of experiments with the slot arrays formed on the same membrane. Using a force laser power of 1 mW, we scanned the membrane to obtain the deflection as a function of incident laser position on the membrane, obtaining the lock-in amplifier results shown in Fig. 4. These data allowed location of the center
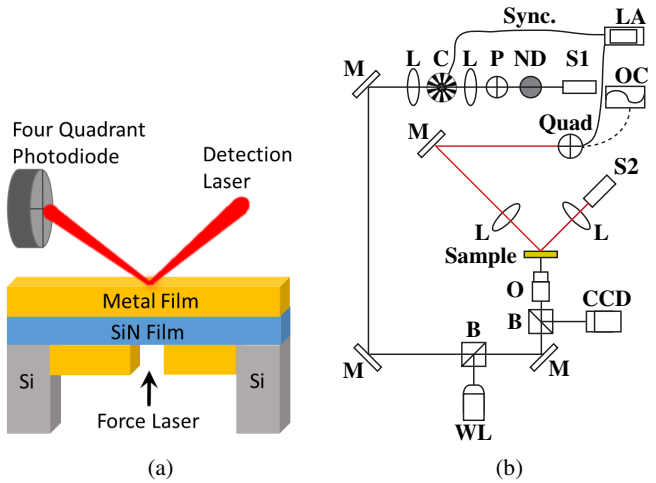
FIG. 3. (a) The measurement of deflection uses a quadrant detection system, allowing monitoring of the deflection due to the chopped 1070 nm force laser (polarized with magnetic field out of the page). (b) Schematic for the experiment. S1: 1070 nm cw fiber force laser (IPG photonics YLR-10-AC), S2: 640 nm sensing laser (Coherent StingRay), quadrant photodiode (Quad) (OSI Optoelectronics SPOT 9D-MI) with 640 nm bandpass filter and amplifier (OnTrak OT-301), oscilloscope (OC), lock-in amplifier (LA) (Zurich Instruments HF2), neutral density filter (ND), white light source (WL), polarizer (P), chopper (C), objective lens (O), silver mirror (M), beam splitter (B), lens (L), charge coupled device (CCD) camera. The membrane structure location was adjusted using a computer-controlled X-Y stage.

of the slot arrays based on the local maximum deflection. With the center of the slot arrays determined, we measured the total deflection with illumination at the center of each slot array and the symmetric planar surface point, as a function of incident laser power. The deflection direction information from the lock-in amplifier phase data was verified at the four symmetric positions with an oscilloscope. The solid circle points in Fig. 5(a) show the measured (total) deflection and the dotted lines are a least mean square error fit for optical powers less than 1 mW,
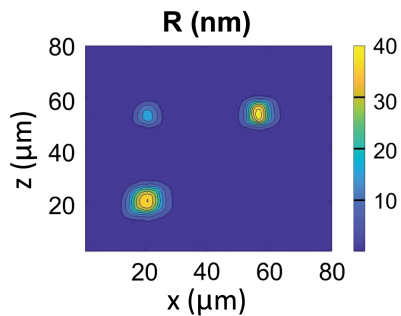

FIG. 4. Scanned membrane deflection magnitude (R) as a function of incident laser position with 1 mW force laser power. The location of the three slot arrays is clearly visible. The orientation of the three slot arrays differs from that in Fig. 2(a) because the sensing laser is on the opposite side of the membrane to the slots and the perspective of the SEM image.

selected so that all of the data are in the small signal, linear regime (with respect to force laser power). The dotted lines are treated as the measured data for the three slot arrays and the planar surface. All four measurement locations on the membrane have the same deflection direction, towards the sensing laser side (and in the direction of the incident force laser). The total deflection in Fig. 5(a) for the strong push case is largest, followed by the weak push, strong pull, and, far smaller, the planar case. The strong pull total deflection is less than the weak push because the optical force is in the opposite direction to the thermally-driven deflection. The measurement error bars (that are more pronounced in the expanded view) were determined based on 100 measurements with the lock-in amplifier (4th-order filter,
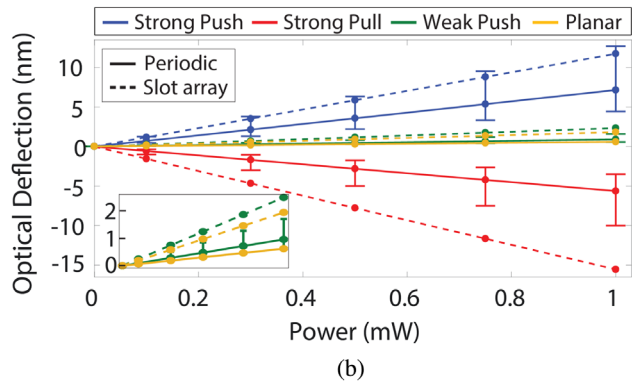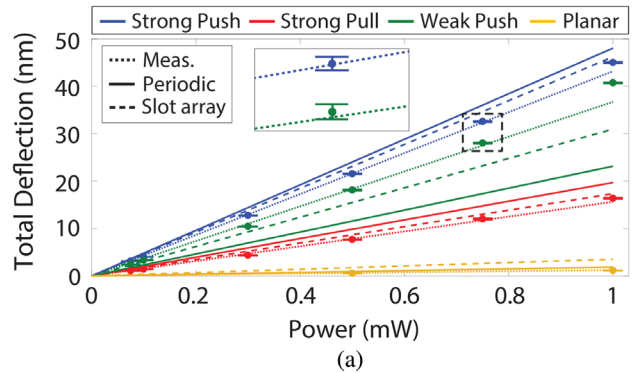

FIG. 5. (a) Measured (solid circles) and fitted and predicted (lines) total deflection as a function of incident laser power: enhanced pushing force (blue), enhanced pulling force (red), weak pushing force (green), and planar surface (yellow). Inset: enlargement of the dashed square region showing measurement error bars. Dotted: fits to the measured data; dashed: fits from a simulation with a Gaussian beam incident on each slot array; and solid: fits from a simulation with plane wave illumination of the corresponding periodic structures using the measured mean slot width and period. (b) Extracted optical deflection: dashed lines are from the exact slot array structures; solid lines are from the periodic structure simulations. The error bars describe sensitivity to structure using the means and standard deviations of the slot arrays from the SEM images (and are not the extraction errors). The inset shows expanded scale data. The blue curves for a large pushing force show about an order or magnitude increase in pressure relative to the planar surface (yellow).

bandwidth of 1.46 Hz, 899 samples/s with an interval of 1.11 ms at the output of the lock-in filter, and a 10 ms delay between individual samples collected with a LabVIEW program, resulting in a total of 100 samples), and are found to be negligible for our purposes.

The total deflection in Fig. 5(a) has contributions from both the direct optical force and heating. In the small displacement regime, the total deflection is linearly related to optical force and heating and can be described as a superposition of direct optical deflection and thermally-driven deflection. Both terms in Eq. (2) contribute to the direct optical force. An additional force contribution is needed to describe thermally-driven deflection, which is a result of optical absorption. We generate the simulated optical force from Eq. (2) and the dissipated power from optical absorption for each slot structure and the planar membrane using the respective numerical field solutions. Fitting parameters are used to relate the calculated optical force to deflection, α m/N, and the thermal dissipation to deflection, β m/W, resulting in a decomposition of the total deflection as $\mathbf{D} = \alpha\mathbf{F} + \beta\mathbf{T}$. Here, $\mathbf{D}$ is a vector of measured total displacements (the data for the three slot array structures and the planar case), $\mathbf{F}$ is a vector whose entries are the corresponding simulated optical forces from Eq. (2), and the vector $\mathbf{T}$ contains the simulated total dissipated power for each. The first term ($\alpha\mathbf{F}$) presents the deflection due to the optical force and the second term ($\beta\mathbf{T}$) that from optical absorption and hence heating. We use the dotted line fits in Fig. 5(a) to form $d\mathbf{D}/dP_o$ (a 4×1 vector), with P_o the variable force laser power, and then a least squares fit to estimate a single α and β for $d\mathbf{F}/dP_o$ and $d\mathbf{T}/dP_o$, respectively, that hold for all structures. The accuracy of this procedure is clear in predicting all experimental data, as shown in the deflection results of Fig. 5(a).

Figure 5(a) shows the results with two modeling approaches: a simple 2D periodic structure assumed for each slot array with plane wave illumination (solid), and a more accurate 3D Gaussian beam illumination of each slot array with a sequence of 2D slice solutions accounting for the beam profile along the length of the slots (dashed). The fields and force densities for each finite-width structure with a Gaussian incident field ($1/e$ field at a beam half-width of 7 μm) were found to have similar key features to the 2D periodic case with plane wave illumination. The 2D slice approximation of the 3D solution was investigated by calculating the 3D force and dissipation on a planar (Au-SiN-Au) surface by comparing with results from a superposition of 2D slices, and found to be satisfactory. The simulated results use the experimentally derived α and β to relate calculated force and dissipation, respectively, to displacement. The simulated total deflection results using the periodic assumption (with the mean width and period of each array) compare favorably with those for each slot array with Gaussian beam illumination. All simulated results in Fig. 5(a) are sufficiently close to the measured data to make conclusions regarding extracted optical force deflection and related enhancement of the pressure.

The extracted optical deflection results as a function of incident optical power are shown in Fig. 5(b). The dashed lines are the results using the more accurate slice model with the measured Gaussian beam profile. The mean values of each slot width and separation for each array were obtained from the SEM images and used to obtain the simulated results (with the extracted α and β). The substantial differences between the large pushing force and pulling force deflections and the planar results represent the force enhancement. In order to appraise sensitivity of the extraction to geometry variations, we pursued a statistical study, and those results are shown by the solid lines in Fig. 5(b) that have associated error bars. It should be emphasized that the resulting error bars are not the errors in determining the slot array parameters, but are an indication of sensitivity of the method for determining optical force deflection to gross variations in the geometry, should there have been factors of which we were unaware. From the SEM images, we obtained a mean and a standard deviation for each array slot width and period (see the caption of Fig. 2). Using the geometry means and the means plus and minus the standard deviations, we calculated the optical force and power dissipation and repeated the least squares fitting process with all the combinations of slot widths and separations for the different sets of slots, using the simple plane wave model. We determined the standard deviations of the fitted optical deflections and plot these as the error bars in Fig. 5(b). The error bars are asymmetric because the points and lines were determined using the geometry means, and the means from the statistical treatment are not identical. Note that even with this rather artificial and extreme set of variations in the extracted optical deflection, all results in Fig. 5(b) are distinct and clearly demonstrate an increase in deflection based upon slot structure, relative to the planar case. Importantly, Fig. 5(b) shows a force on the structured Au film, in the case of the large push force (blue), that is approximately an order of magnitude higher than that on the planar Au surface (yellow).

We have demonstrated an enhanced optical force on a metallic surface that depends on its nanostructured features. The increase in optical pressure therefore results from optical field interaction with the material in the third dimension. The general principle is that an asymmetric cavity-enhanced field increase, associated with a resonance, leads to an increase in the force density within the material and hence to a substantial increase in the total force, relative to the planar case. Control of the scattered field in the structured material can regulate both the force magnitude and direction, and allow a negative pressure. The interplay between material structured at the nanometer scale and optical force will have substantial consequences in applications that include all-optical communication,

remote actuation, propulsion, and biophysics. For example, in all-optical communication, optical signals could be used to move a structure that would then select a different optical (network) path [22,23]. Remote actuation would be enhanced by greater sensitivity and control of the force direction, both of which might benefit cavity cooling [24,25]. Regulation and enhancement of optical forces with structured material should prove interesting in the field of cavity optomechanics [26,27]. Also, by structuring beads used in optical tweezer experiments related to biomolecules, more control becomes available [6]. Finally, nanostructured media provides an important dimension with regard to thermomechanical structures, where light is used to heat and deform metal films [28].

*Corresponding author.
 webb@purdue.edu

[1] P. Lebedev, Ann. Phys. (Berlin) **311**, 433 (1901).
[2] E. F. Nichols and G. F. Hull, Phys. Rev. **17**, 26 (1903).
[3] J. C. Maxwell, *A Treatise on Electricity and Magnetism* (Dover, New York, 1954), Vol. 2.
[4] A. Ashkin and J. M. Dziedzic, Phys. Rev. Lett. **30**, 139 (1973).
[5] A. Ashkin, J. M. Dziedzic, J. E. Bjorkholm, and S. Chu, Opt. Lett. **11**, 288 (1986).
[6] J. R. Moffitt, Y. R. Chemla, S. B. Smith, and C. Bustamante, Annu. Rev. Biochem. **77**, 205 (2008).
[7] D. J. Wineland and W. M. Itano, Phys. Rev. A **20**, 1521 (1979).
[8] C. J. Myatt, E. A. Burt, R. W. Ghrist, E. A. Cornell, and C. E. Wieman, Phys. Rev. Lett. **78**, 586 (1997).
[9] W. D. Phillips, Rev. Mod. Phys. **70**, 721 (1998).
[10] A. H. Velzen and K. J. Webb, Phys. Rev. B **92**, 115416 (2015).
[11] G. K. Campbell, A. E. Leanhardt, J. Mun, M. Boyd, E. W. Streed, W. Ketterle, and D. E. Pritchard, Phys. Rev. Lett. **94**, 170403 (2005).
[12] K. J. Webb and Shivanand, Phys. Rev. E **84**, 057602 (2011).
[13] M. Mansuripur, A. R. Zakharian, and E. M. Wright, Phys. Rev. A **88**, 023826 (2013).
[14] K. J. Webb, Phys. Rev. Lett. **111**, 043602 (2013).
[15] A. Einstein and J. Laub, Ann. Phys. (Berlin) **331**, 541 (1908).
[16] K. J. Webb, Phys. Rev. B **94**, 064203 (2016).
[17] COMSOL, Comsol multiphysics modeling software, http://www.comsol.com.
[18] P. B. Johnson and R.-W. Christy, Phys. Rev. B **6**, 4370 (1972).
[19] See Supplemental Material at http://link.aps.org/supplemental/10.1103/PhysRevLett.122.083901 for details on the field and force density simulations.
[20] A. Novitsky, C.-W. Qiu, and H. Wang, Phys. Rev. Lett. **107**, 203601 (2011).
[21] J. Canny, IEEE Trans. Pattern Anal. Mach. Intell. **8**, 679 (1986).
[22] J. Rosenberg, Q. Lin, and O. Painter, Nat. Photonics **3**, 478 (2009).
[23] D. Nikolova, S. Rumley, D. Calhoun, Q. Li, R. Hendry, P. Samadi, and K. Bergman, Opt. Express **23**, 1159 (2015).
[24] S. Gigan, H. R. Böhm, M. Paternostro, F. Blaser, G. Langer, J. B. Hertzberg, K. C. Schwab, D. Bäuerle, M. Aspelmeyer, and A. Zeilinger, Nature (London) **444**, 67 (2006).
[25] A. Schliesser, P. Del'Haye, N. Nooshi, K. J. Vahala, and T. J. Kippenberg, Phys. Rev. Lett. **97**, 243905 (2006).
[26] A. Dorsel, J. D. McCullen, P. Meystre, E. Vignes, and H. Walther, Phys. Rev. Lett. **51**, 1550 (1983).
[27] T. J. Kippenberg, H. Rokhsari, T. Carmon, A. Scherer, and K. J. Vahala, Phys. Rev. Lett. **95**, 033901 (2005).
[28] H. Zhu, F. Yi, and E. Cubukcu, Nat. Photonics **10**, 709 (2016).